Stable Open-Shell Phosphorane Based on a Redox-Active Amidodiphenoxide Scaffold

Citation: Pistner, Allen J. et al. "Stable Open-Shell Phosphorane Based on a Redox-Active Amidodiphenoxide Scaffold." Inorganic Chemistry 56, 15 (June 2017): 8661–8668 © 2017 American Chemical Society

As Published: http://dx.doi.org/10.1021/acs.inorgchem.7b00657

Publisher: American Chemical Society (ACS)

Persistent URL: http://hdl.handle.net/1721.1/117203

Version: Author's final manuscript: final author's manuscript post peer review, without publisher's formatting or copy editing

A Stable Open-Shell Phosphorane based on a Redox Active Amidodiphenoxide Scaffold

Allen J. Pistner,[‡] Hye Won Moon,[†] Alexey Silakov,[‡] Hemant P. Yennawar[‡,§] and Alexander T. Radosevich*[,†]

[†] Department of Chemistry, Massachusetts Institute of Technology, Cambridge, Massachusetts 02139

[‡] Department of Chemistry, The Pennsylvania State University, University Park, Pennsylvania 16802

[§] X-ray Crystallography Laboratory, Department of Biochemistry and Molecular Biology, The Pennsylvania State University, University Park, Pennsylvania 16802

Supporting Information Placeholder

ABSTRACT: The synthesis and redox reactivity of pentacoordinate phosphorus compounds incorporating a redox active *ONO* amidodiphenoxide scaffold (*ONO* = *N*,*N*-bis(3,5-di-*tert*-butyl-2-phenoxide)amide) are described. Dichloro- and diphenylphosphoranes, **2**•Cl$_2$ and **2**•Ph$_2$ respectively, are synthesized and crystallographically characterized. Cyclic voltammograms of **2**•Cl$_2$ show only a single irreversible oxidation (E_{pa} = +0.83 V vs $Cp_2Fe^{o/+}$), while the diphenyl analogue **2**•Ph$_2$ is reversibly oxidized at lower applied potential ($E_{1/2}$ = +0.47 V vs $Cp_2Fe^{o/+}$). Chemical oxidation of **2**•Ph$_2$ with AgBF$_4$ produces the corresponding radical cation [**2**•Ph$_2$]$^{\bullet+}$, where EPR spectroscopy and DFT calculations reveal that the unpaired spin density is largely ligand based and is highly delocalized throughout the *ONO* framework of the paramagnetic species. The solid state structures indicate only minor geometrical changes between the neutral **2**•Ph$_2$ and oxidized [**2**•Ph$_2$]$^{\bullet+}$ species, consistent with fast self-exchange electron transfer as observed by NMR line-broadening experiments.

INTRODUCTION

Interest in molecular inorganic compounds with redox active ligand scaffolds has been increasing because the distribution of redox properties across both metal and ligand alters the density and nature of frontier electronic states.[1] Such cooperative redox reactivity presents opportunities for new multielectron transformations.[2-5] Catalysts employing redox active ligands continue to make significant advances in synthetic chemistry and have been the subject of several recent reviews.[6-10]

Among the most actively investigated redox-active scaffolds has been the *ONO* chelate *N*,*N*-*bis*(3,5-di-*tert*-butyl-2-phenoxide)amide **A**. Prepared initially as a binding fragment for heavy main group metals by Stegmann and Scheffler,[11-13] compound **A** exhibits a rich chelating chemistry for diverse transition metal and main group elements.[14-29] Chief among the findings in such studies is the propensity of the *ONO* fragment to support several discrete redox states as depicted in Figure 1: closed-shell trianionic **A**, open-shell dianionic semiquinonate **B**, and monoanionic quinonate **C**. Access to each of these electronic states may be controlled not only on the identity of the chelated element, but also by external reagents in such a way as to permit catalysis involving reversible interconversion of several or all of these electronic configurations.[30]

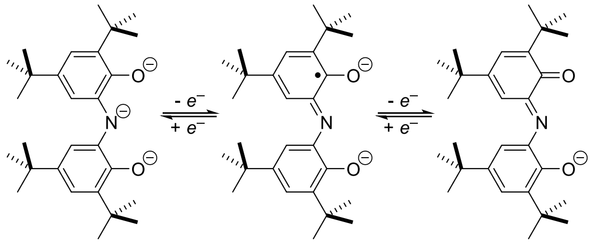

A **B** **C**

Figure 1. Redox states of the amidodiphenoxide *ONO* scaffold **A**–**C**.

We have been investigating the chemistry of phosphorus compounds supported within heteroatom-based trianionic binding motifs. For instance, we have reported on both *ONO*- and *NNN*-supported phosphorus compounds that undergo intermolecular oxidative addition of E–H bonds (E = O, N), in some cases reversibly.[31,32] Aldridge and Goicoechea have subsequently reported in a similar vein with phosphorus compounds based on supporting structure **A**.[33,34] Many structurally related neutral phosphoranes in this series are known, especially from the studies of Contreras and workers.[35] Despite the well-known redox reactivity of **A**–**C**, the preparation of phosphorus compounds incorporating the *ONO* fragment in its open shell electronic configuration **B** has not been demonstrated explicitly to date.

In the interest of better understanding the interplay between phosphorus(V) and *ONO* ligand electronic states, we describe here the synthesis, structural and electronic properties of several closed- and open-shell phosphorus compounds based on the *N*,*N*-*bis*(3,5-di-*tert*-butyl-2-phenoxide)amide chelate. We demonstrate the redox activity of *ONO*-supported phosphoranes through electrochemical and chemical oxidation and characterize the extent of electron-hole delocalization through EPR spectroscopic and DFT theoretical methods Our results are consistent with the presence of accessible and reversible ligand centered oxidation events in these compounds, suggesting a possible role in future reactivity studies.

RESULTS AND DISCUSSION

Synthesis and Structure of Closed-Shell Phosphoranes. Investigation was initiated with the preparation of two related closed-shell phosphoranes with varying substituents at phosphorus (Figure 2). The synthesis began with the preparation of homoleptic zinc complex **1** from the multicomponent self-assembly reaction of $Zn(OAc)_2$, 3,5-di-*tert*-butylcatechol and ammonia following the procedure of Girgis and Balch.[36] From **1**, phosphoranes **2**•Cl_2 and **2**•Ph_2 can be accessed directly by treatment with trichlorophosphine (PCl_3) and chlorodiphenylphosphine ($PClPh_2$), respectively, in a modification of the synthetic procedure previously reported by Contreras and coworkers.[32] The ^{31}P NMR chemical shift for each species falls in the range expected for pentacoordinated phosphorus ($\delta_{2\bullet Cl_2}$ = –20.1 ppm; $\delta_{2\bullet Ph_2}$ = –27.9 ppm). In effect, the addition of the tricoordinate phosphorus reagents to **1** results in formal reduction of the ONO ligand from its iminoquinone oxidation state (*cf.* **C**) to the trianionic amidodiphenoxide state (*cf.* **A**) with formal oxidation of the phosphorus center to the P(V) oxidation state. Both **2**•Cl_2 and **2**•Ph_2 are prepared in high yield according to this route (73% and 79%, respectively).

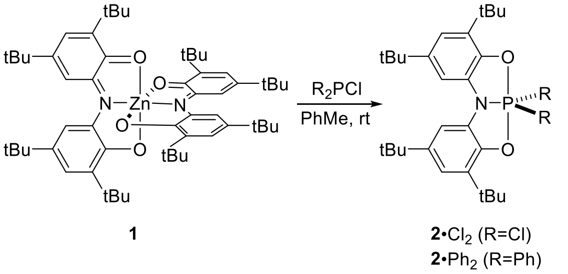

Figure 2. Synthesis of **2**•Cl_2 and **2**•Ph_2.

Single crystals of **2**•Ph_2 were obtained by slow evaporation of an acetonitrile/methylene chloride solution, and the structure of **2**•Ph_2 was elucidated by X-ray diffraction analysis. As depicted in the thermal ellipsoid plot in Figure 3, compound **2**•Ph_2 exhibits a trigonal bipyramidal geometry (τ = 0.85), with the phenyl fragments occupying two basal sites and the *ONO* fragment spanning the remaining one basal and two apical positions. Selected bond lengths and angles are collected in Table 1. The phosphorus and three basal substituents are effectively coplanar, with the sum of the angles about phosphorus $\Sigma\angle X–P_1–Y$ = 360.02°. Within this plane, the bond angles $\angle N_1–P_1–C_1$ and $\angle N_1–P_1–C_7$ were measured to be 122.37(8)° and 123.59(9)°, respectively, while the $\angle C_1–P_1–C_7$ is slightly compressed at 114.04(10)°. The oxygen substituents are only modestly deformed away from rigorously diapical positions by the tridentate chelating motif (bond angle $\angle O_1–P_1–O_2$ = 174.72(6)°). Bond lengths $d(O_1–P_1)$ and $d(O_2–P_1)$ exhibit a slight dissymmetry (1.6985(18) Å and 1.7048(18) Å, respectively) but otherwise fall within the expected range of oxygen-phosphorus distances in pentacoordinated phosphorus. The $N_1–P_1$ bond was found to be of similar length (1.699(2) Å) as the O–P bonds, whereas the carbon-phosphorus bonds to the phenyl are somewhat longer at 1.807(2) Å and 1.800(2) Å for $d(C_1–P_1)$ and $d(C_7–P_1)$, respectively.

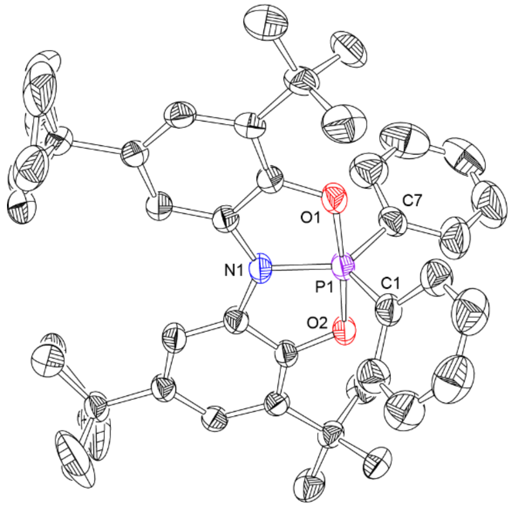

Figure 3. Solid state structure of **2**•Ph_2. Thermal ellipsoids shown at 50% probability with the hydrogens atoms omitted for clarity.

*Electrochemistry of Phosphoranes **2**•Cl_2 and **2**•Ph_2.* A cyclic voltammogram of **2**•Cl_2 in dichloromethane (1.0 mM analyte, 0.1 M nBu_4NPF_6 supporting electrolyte, T = 293 K, scan rate = 100 mV/s, glassy carbon working electrode) shows an electrochemically irreversible wave in the positive sweep with anodic peak potential E_{pa} = +0.83 V vs $Cp_2Fe^{o/+}$ (Figure 4, *top*). By contrast, a cyclic voltammogram of **2**•Ph_2 under identical experimental conditions shows the presence of a reversible first oxidation event at less positive potentials $E_{1/2}$ = +0.47 V vs $Cp_2Fe^{o/+}$ (Figure 4, *bottom*).

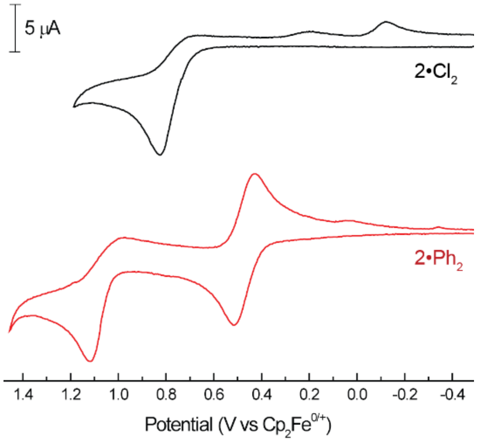

Figure 4. Cyclic voltammograms of **2**•Cl_2 (*black*) and **2**•Ph_2 (*red*) recorded in CH_2Cl_2 solution (1.0 mM analyte, 0.1 M NBu_4PF_6 supporting electrolyte, scan rate 100 mV/s, glassy carbon working electrode).

It is evident that the identity of the basal substituent exerts a controlling effect on the electrochemical behavior of phosphoranes **2**•Cl_2 and **2**•Ph_2. Inductive effects presumably are largely responsible for modulating the redox potential of **2**•Cl_2 and **2**•Ph_2 over ca. 360 mV. Differential strengths and kinetic stabilities of basal P–Cl and P–C bonds account for the observed (ir)reversibility of the voltammograms. We note that at more positive applied potentials, a second irreversible oxidation event is evident for **2**•Ph_2 (E_{pa} = +1.12 V vs $Cp_2Fe^{o/+}$); the nature of this oxidation remains the topic of ongoing investigation.

*Chemical Oxidation of Phosphorane **2**•Ph_2.* Given the reversibility of the electrochemical response of **2**•Ph_2, we wished to investigate the possibility of isolating the open-shell product of one electron oxidation. Consistent with the cyclic voltammetry, treatment of **2**•Ph_2 with the single electron oxidant silver tetrafluoroborate in CH_2Cl_2 (E_o = +0.65 V vs $Cp_2Fe^{o/+}$)[37] results in a rapid change in color from a clear solution to dark blue and deposition of elemental Ag. These solutions are metastable at room temperature over the course days, but undergo slow decomposition to ill-defined products especially upon concentration. By contrast, stable samples suitable for isolation in single crystalline form may be obtained with noncoordinating barfate anion $BAr^F{}_4{}^-$=$B[C_6H_3\text{-}3,5\text{-}(CF_3)_2]_4{}^-$ as the counterion.

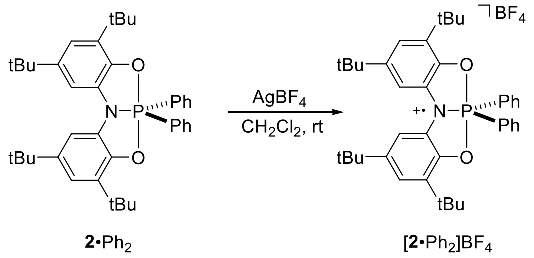

Figure 5. Chemical oxidation of **2**•Ph_2 with $AgBF_4$.

The solid state structure of the resulting [**2**•Ph_2]BAr^F (obtained as a pentane solvate) was elucidated through x-ray crystallography and is displayed in Figure 6. To a first approximation, the chemical oxidation **2**•$Ph_2 \rightarrow$ [**2**•Ph_2]$^{\bullet+}$ results in only minor global structural changes; Figure 7 depicts a wire-frame overlay of the experimentally determined structures **2**•Ph_2 (*green*) and [**2**•Ph_2]$^{\bullet+}$ (*red*) demonstrating that both compounds present qualitatively similar local structures about the phosphorus center. Upon closer inspection, though, several noteworthy structural aspects are discernable (see Table 1 for selected bond lengths and angles). A slight apparent distortion from an idealized trigonal bipyramid toward a square pyramidal structure (τ = 0.54) is apparent; this distortion is associated with slight folding of the *ONO* supporting structure as given by $\angle O_1\text{–}P_1\text{–}O_2$ = 166.7(1)° ($\Delta_{\mathbf{2}\bullet Ph_2{}^{0/\bullet+}}$ = –8.0°), and a rocking of the two phenyl moieties such that $\angle N_1\text{–}P_1\text{–}C_1$ = 134.2(1)° ($\Delta_{\mathbf{2}\bullet Ph_2{}^{0/\bullet+}}$ = +11.8°) and $\angle N_1\text{–}P_1\text{–}C_7$ = 111.9(1)° ($\Delta_{\mathbf{2}\bullet Ph_2{}^{0/\bullet+}}$ = –11.7°). Attending these changes in bond angles, several differences are also observed in bond lengths. While both $P\text{–}C_{phenyl}$ bond lengths do not change, $d(C_1\text{–}P_1)$ = 1.810(3) Å ($\Delta_{\mathbf{2}\bullet Ph_2{}^{0/\bullet+}}$ = +0.003Å) and $d(C_7\text{–}P_1)$ = 1.805(4) Å ($\Delta_{\mathbf{2}\bullet Ph_2{}^{0/\bullet+}}$ = +0.005Å), the bond distances from phosphorus to nitrogen and one oxygen of the *ONO* heteroatoms increase. The most significant change occurs to the diarylamido nitrogen, where $d(N_1\text{–}P_1)$ = 1.786(3) Å ($\Delta_{\mathbf{2}\bullet Ph_2{}^{0/\bullet+}}$ = +0.09Å). Along with this change, there is an apparent increase in the quinoidal character of the *ONO* fragment; the $N_1\text{–}C_{ipso}$ bond distances, which had been nearly identical in **2**•Ph_2 (1.397(2) Å and 1.394(2) Å), are noticeably dissymmetric in [**2**•Ph_2]$^{\bullet+}$ (1.391(4) Å and 1.365(3) Å). From these data, it is apparent that single electron oxidation of **2**•Ph_2 results in subtle yet discernable metrical changes in structure, both locally in the immediate binding environment of phosphorus and also throughout the *ONO* framework.

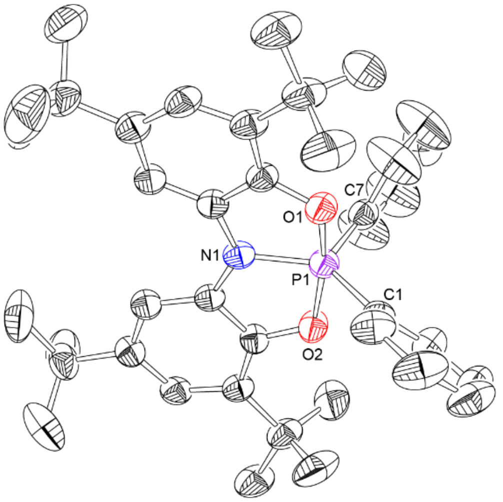

Figure 6. Solid state structure of the open-shell phosphorane **2**•$Ph_2{}^{\bullet+}$. Thermal ellipsoids shown at 50% probability with the $B[3,5\text{-}(CF_3)\text{-}C_6H_3]_4{}^-$ counter ion, a disordered pentane solvent molecule, and hydrogen atoms omitted for clarity.

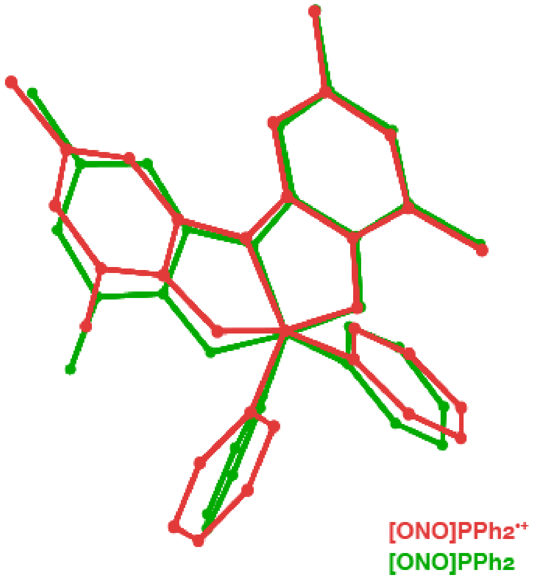

Figure 7. Wire frame overlay of the solid state structures for **2**•Ph_2 (*green*) and [**2**•Ph_2]$^{\bullet+}$ (*red*). Methyl groups, hydrogen atoms, and counterions omitted for clarity.

Table 1. Selected bond lengths (Å) and angles (°) for 2•Ph$_2$ and [2•PPh$_2$]$^{•+}$.

Metric	**2**•Ph$_2$	[**2**•PPh$_2$]$^{•+}$.
C_1–P_1	1.807(2)	1.810(3)
C_7–P_1	1.800(2)	1.805(4)
N_1–P_1	1.699(2)	1.786(3)
O_1–P_1	1.6985(18)	1.693(2)
O_2–P_1	1.7048(18)	1.736(2)
C_7–P_1–C_1	114.04(10)	113.7(1)
O_1–P_1–N_1	87.55(7)	86.1(1)
O_1–P_1–O_2	174.72(6)	166.7(1)
O_2–P_1–N_1	87.46(7)	85.3(1)
N_1–P_1–C_1	122.37(8)	134.2(1)
N_1–P_1–C_7	123.59(9)	111.9(1)

*Spectroscopic and Computational Investigations of [**2**•Ph$_2$]BF$_4$.* The absorption profile for each of the three compounds **2**•Cl$_2$, **2**•Ph$_2$, and [**2**•Ph$_2$]BF$_4$ was recorded using UV-vis spectroscopy, as shown in Figure 8. The compound **2**•Cl$_2$ displayed a single absorption centered at λ_{max}= 285 nm; the high-energy of this transition is not unexpected for a closed-shell phosphorane species. Similarly, the neutral diphenyl phosphorane **2**•Ph$_2$ displayed a similar absorption profile with a single absorption band slightly to the red at λ_{max} = 307 nm. By contrast, the absorption profile of the open shell species [**2**•Ph$_2$]BF$_4$ exhibits several lower energy features; a broad absorption centered at 665 nm with a shoulder appearing at 617 nm is apparent in the visible region of the spectrum, with additional absorptions at 354 nm and 371 nm.

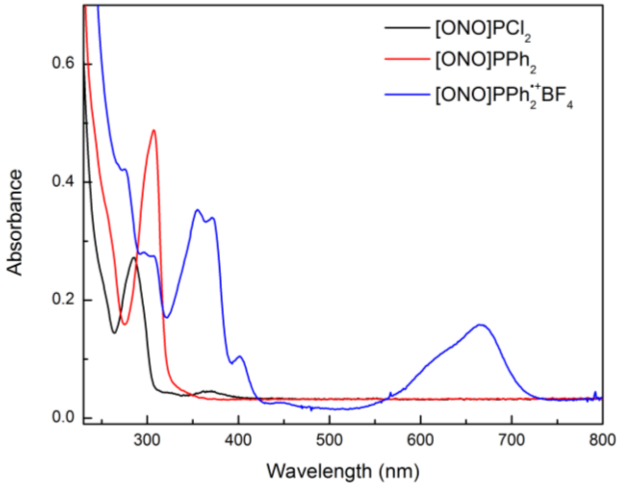

Figure 8. UV-vis absorption spectra recorded for **2**•Cl$_2$ (*black*, 20 μM in CH_2Cl_2), **2**•Ph$_2$ (*red*, 20 μM in CH_2Cl_2), and [**2**•Ph$_2$]BF$_4$ (60 μM in CH_2Cl_2) at ambient temperature.

The paramagnetic complex [**2**•Ph$_2$]BF$_4$ was further probed with the use of EPR spectroscopy; the experimental spectrum as well as a simulated spectrum are displayed in Figure 9. The room temperature, solution phase (CH_2Cl_2) EPR spectrum of [**2**•Ph$_2$]BF$_4$ displays spectral envelope centered at g=2.006, with an apparent 9-line coupling pattern. The observed splitting was interpreted by accounting for two pairs of equivalent ^{1}H nuclei with isotropic hyperfine coupling constants of 9.2 MHz and 2.1 MHz; a ^{14}N hyperfine coupling constant of 13.4 MHz, and a ^{31}P hyperfine coupling constant of 43.5 MHz. Both the *g*-value and the extracted hyperfine coupling indicate extensive delocalization of the spin density onto the *ONO* ligand scaffold. Substantial hyperfine coupling of the two pairs of equivalent ^{1}H nuclei indicates equal distribution of spin density over the two phenyl moieties of the *ONO* ligand scaffold. The observed ^{31}P hyperfine coupling constant is seemingly large, however we note that it is at least an order of magnitude smaller than typical value for phosphorus-centered radicals[38,] and thus indicate rather small unpaired spin population on this atom.

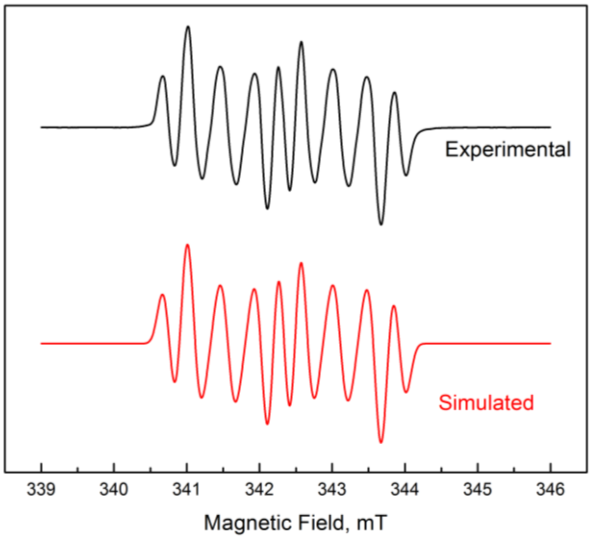

Figure 9. (*black*) X-band EPR spectra (9.61 GHz) of [**X**•Ph$_2$]BAr^F in CH_2Cl_2 at 293 K. (*red*) Simulated spectrum with hyperfine fitting parameters as shown in Table 2.

Density functional theory (DFT) calculations were performed to gain further insight into the molecular and electronic structure associated with the ligand centered oxidation event. Geometry optimization and electronic structure calculation for [**2**•Ph$_2$]$^{•+}$ using DFT (unrestricted BP86 functional and 6-311+g(d) basis set on all atoms, followed by single point calculation at the B3LYP/def-TZVPP level of theory) were performed using the crystallographically determined X-ray coordinates as an initial guess geometry. The theoretically predicted structure is in good metrical agreement with the experimental structure. The spin density plot for [**2**•Ph$_2$]$^{•+}$ is displayed in Figure 10. The singly occupied molecular orbital (SOMO) shows significant delocalization across the *ONO* supporting framework, indicating that the single electron oxidation of **2**•Ph$_2$ → [**2**•Ph$_2$]$^{•+}$ is almost entirely ligand based. By contrast, the central phosphorus center is found to have little spin density (Mulliken spin population 0.003). Indeed, the hyperfine coupling constants predicted by this spin distribution were found to match closely to those obtained experimentally (Table 2). The spin density distribution obtained resembles the group 14 compounds of the similar scaffold obtained and characterized by Stegmann and Scheffler.[11-13] In all cases, the spin density was found to be largely distributed over the ONO structure. The notable difference is more localized spin density on the peripheral carbons in the current case: ratio A(H-$C_{15,31}$)/A(H-$C_{17,29}$) is about 4.4 for $[\mathbf{2}{\bullet}\mathrm{Ph}_2]^{\cdot+}$ as compared to about 2 for (*ONO*)PbAr_2, (*ONO*)SnAr_2, and (*ONO*)GeAr_2 compounds. This difference in the spin distribution is also apparent from about 30% smaller A(^{14}N) of the central nitrogen (cf. Table S7, Supporting Information).

Table 2. Comparison of experimental (EPR) and calculated (DFT) isotropic hyperfine coupling constants.

Nucleus[a]	Assignment[b]	Experimental[c]	Calculated[c]
^{1}H (2)	C_{15}–H/C_{31}–H	9.2	8.7
^{1}H (2)	C_{17}–H/C_{29}–H	2.1	1.24
^{14}N	N_1	13.4	10.1
^{31}P	P_1	43.5	44.3

[a] Nucleus responsible for observed hyperfine coupling. Parentheses indicated number of equivalent nuclei. [b] Atom labels refer to structure depicted in Figure S2. [c] Values in MHz.

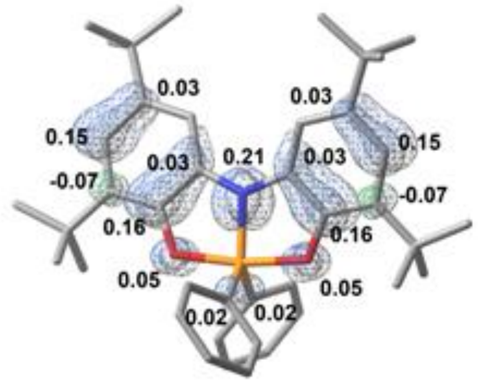

Figure 10. Geometry optimized structure of $[\mathbf{2}{\bullet}\mathrm{Ph}_2]^{\bullet+}$ (B3LYP/def-TZVPP//B86/6-311+g(d)) superimposed with spin density plot (blue - positive density, green - negative density). Relevent Mulliken spin populations are noted.

In view of the small structural changes associated with the oxidation of $\mathbf{2}{\bullet}\mathrm{Ph}_2 \rightarrow [\mathbf{2}{\bullet}\mathrm{Ph}_2]^{\bullet+}$ and the reversibility of this process, we undertook investigations of the rate of electron transfer self-exchange using the method of ^{1}H NMR line-broadening.[39] For a pure sample of closed-shell phosphorane $\mathbf{2}{\bullet}\mathrm{Ph}_2$, a resonance at δ 1.31 ppm is observed for one of the *tert*-butyl groups on the ligand periphery. The line width (determined as the full-width at half-maximum height by spectral fitting of the Lorentzian line shape) is estimated at 4.3(5) Hz. By contrast, the ^{1}H NMR spectrum of $[\mathbf{2}{\bullet}\mathrm{Ph}_2]^{\bullet+}$ shows a very broad resonance at δ 1.74 ppm with an estimated line width of 153(10) Hz. A series of ^{1}H NMR spectra were recorded at room temperature with varying mole fraction of the neutral compound $\mathbf{2}{\bullet}\mathrm{Ph}_2$ and the oxidized species $[\mathbf{2}{\bullet}\mathrm{Ph}_2]^{\bullet+}$ (Table 3). Starting from pure $\mathbf{2}{\bullet}\mathrm{Ph}_2$, increases in the quantity of paramagnetic species $[\mathbf{2}{\bullet}\mathrm{Ph}_2]^{\bullet+}$ causes the *tert*-butyl resonance to shift downfield and broaden. A linear relationship between mole fraction of $[\mathbf{2}{\bullet}\mathrm{Ph}_2]^{\bullet+}$ and chemical shift is observed. The rate constant (k_{ex}) for the electron transfer self-exchange between compound $\mathbf{2}{\bullet}\mathrm{Ph}_2$ and $[\mathbf{2}{\bullet}\mathrm{Ph}_2]^{\bullet+}$ was determined according to eq 1, where χ_d and χ_p represent the mole fraction of $\mathbf{2}{\bullet}\mathrm{Ph}_2$ and $[\mathbf{2}{\bullet}\mathrm{Ph}_2]^{\bullet+}$, respectively; $\Delta\nu$ is the difference in frequencies (Hz) between diamagnetic $\mathbf{2}{\bullet}\mathrm{Ph}_2$ and paramagnetic $[\mathbf{2}{\bullet}\mathrm{Ph}_2]^{\bullet+}$; C_{tot} is the total concentration; w_p and w_d are the line width at half-maximum for pure samples $\mathbf{2}{\bullet}\mathrm{Ph}_2$ and $[\mathbf{2}{\bullet}\mathrm{Ph}_2]^{\bullet+}$, respectively; and w_{pd} is the line width at half-maximum for the mixture.

Table 3. Data for electron self-exchange NMR line-broadening experiments.

χ_d	χ_p	Shift (Hz)	Line Width (Hz)	k_{ex} (x 10^5)
1	0	657.59	4.32	
0.945	0.055	669.28	22.52	1.2
0.886	0.114	681.93	35.94	1.6
0.843	0.157	691.1	48.36	1.5
0.735	0.265	714.05	67.68	1.9
0.403	0.597	785.03	112.48	2.9
0	1	870.97	153.43	

$$k_{ex} = \frac{4\pi\chi_p\chi_d(\Delta\nu)^2}{C_{tot}(w_{pd} - \chi_p w_p - \chi_d w_d)} \quad (1)$$

Averaging the obtained rate constants k_{ex} over the experimental concentration range in Table 3, we estimate the self-exchange rate between compounds $\mathbf{2}{\bullet}\mathrm{Ph}_2$ and $[\mathbf{2}{\bullet}\mathrm{Ph}_2]^{\bullet+}$ at $k_{ex} = 1.8(7) \times 10^5\ \mathrm{M}^{-1}{\bullet}\mathrm{s}^{-1}$. Although it is of note that small changes in the estimated width at half-maximum height can have a dramatic effect upon the precise obtained rate constant, the comparison of the solid state structures of the two compounds nonetheless supports the notion of a rapid electron transfer self-exchange due to only minor structural reorganization.

CONCLUSIONS

The synthesis and study of phosphorus(V) bound within a redox active *ONO* ligand scaffold has been presented. The phosphorus compounds $\mathbf{2}{\bullet}\mathrm{Cl}_2$ and $\mathbf{2}{\bullet}\mathrm{Ph}_2$ can be synthesized in high yields and have been structurally characterized. The electrochemistry of these systems was probed with the use of cyclic voltammetry, with the compound $\mathbf{2}{\bullet}\mathrm{Cl}_2$ showing only a single irreversible oxidation, while the diphenyl phosphorene $\mathbf{2}{\bullet}\mathrm{Ph}_2$ displays a reversible one-electron oxidation event. Compound $\mathbf{2}{\bullet}\mathrm{Ph}_2$ was chemically oxidized with silver salts to form the radical cation, $[\mathbf{2}{\bullet}\mathrm{Ph}_2]^{\bullet+}$. EPR spectroscopy and DFT calculations revealed that the unpaired spin density in $[\mathbf{2}{\bullet}\mathrm{Ph}_2]^{\bullet+}$ is largely ligand based and is highly delocalized throughout the *ONO* supporting framework of the paramagnetic species. The solid state structures and self-exchange NMR line-broadening experiments indicate that the electron transfer is swift with only modest metrical changes between the neutral and oxidized species.

EXPERIMENTAL SECTION

Methylene chloride (CH_2Cl_2), pentane and toluene were dried according to the method of Grubbs[40] as modified by Bergman[41]. All commercially available reagents were purchased from suppliers and used without further purification. All reactions were carried out under nitrogen either in a double port glovebox (Innovative Technology) or with a Schlenk manifold vented through an oil bubbler unless otherwise noted. All glassware was oven-dried at 120 °C prior to use. Zn complex **1**,[33] and AgBAr^{F}[42] were synthesized according to previous reports. Mass spectrometric data were obtained from the University of Illinois Mass Spectrometry Lab. Elemental analysis data was obtained from Midwest Microlab, Indianapolis, IN.

Spectroscopic Methods. ^{1}H, ^{13}C, and ^{31}P NMR spectra were recorded with a Bruker AV-360, DRX-400 or AV-3-500 spectrometers. $CDCl_3$ and CD_2Cl_2 were purchased from Cambridge Isotopes Laboratories and stored over activated 4 Å molecular sieves in the glovebox prior to use. ^{1}H and ^{13}C NMR spectra were referenced to residual proto-solvent resonances (chloroform 7.26 ppm; 77.16 ppm). ^{31}P NMR spectra were referenced to an external standard (H_3PO_4 0.0 ppm). EPR spectra were recorded using a Bruker ESP300 equiped with ER041MR MW bridge and a ER 4116DM dual mode resonator. The EPR spectrum was recorded using the following settings: MW power = 0.02 mW, MW frequency = 9.6122 GHz, sweep width = 80.0 G, modulation amplitude = 0.2 G, conversion time = 40.96 ms, and time constant = 40.96 ms. EPR simulation was performed utilizing the "garlic" routine from EasySpin for MatLab[43] and aided by a home-written automatic spectral fitting routine. The UV-vis spectroscopy was performed using a Cary 500 spectrometer with analyte solutions prepared using dichloromethane as the solvent. The UV-vis spectrum of [**2**•Ph_2]BF_4 was acquired using dichloromethane that was freshly distilled from CaH_2 and a quartz cuvette that had been silylated using TMS–Cl (5% by volume solution in dichloromethane), rinsed (3x dichloromethane) and dried thoroughly in an oven.

Electrochemistry. All electrochemistry experiments were performed using a Pine WaveNow XV potentiostat. Cyclic voltammetry was performed at ambient temperature in a nitrogen filled glove box using a standard three-electrode configuration. CV scans were recorded using a glassy carbon working electrode (3.0 mm diameter), platinum mesh as the counter electrode and a silver wire separated by a porous Teflon tip and submerged in $TBAPF_6$ solution (0.1 M) as a quasi-reference electrode. The phosphorus analytes (1.0 mM) were prepared in dichloromethane with tetrabutylammonium hexafluorophosphate (0.1 M) as the supporting electrolyte. Sublimed ferrocene (1.0 mM) was added at the end of each experiment as the internal reference.

Electron Self Exchange. ^{1}H NMR spectra were acquired in CD_2Cl_2 on a Bruker AV-3-500 spectrometer at 298 K. The samples were prepared in a nitrogen filled glovebox and from stock solutions of each analyte (25 mM in CD_2Cl_2) in varying ratios for a total volume of 0.5 mL. The mole fractions, chemical shifts and experimental values for the peaks widths (*W*) are displayed in Table 2. The peak widths were determined by Lorentzian line-fitting using the MestReNova 10 software.

X-ray Diffraction Methods. Single crystals of **2**•Ph_2 and [**2**•Ph_2]($B[C_6H_3\text{-}3,5\text{-}(CF_3)_2]_4$) were selected and mounted on a loop using paratone oil on a Bruker SMART APEX diffractometer. The crystal was kept at 213 K during data collection. Using Olex2[44], the structure was solved with the ShelXS[45] structure solution program using Direct Methods and refined with the XL refinement package using Least Squares minimization.

Computational Methods. Density functional theory (DFT) calculations were performed using Gaussian 09 package[46]. Geometry of the oxidized compound was obtained by gas-phase geometry optimization using unrestricted BP86 functional and 6-311+G(d) basis set on all atoms. Starting coordinates were extracted from the crystal structure of **2**•Ph_2. To aid geometry optimization, rotation of all methyl groups was restricted by freezing one of the associated HC-CC dihedral angles. Subsequently, single point gas-phase calculations were performed utilizing unrestricted B3LYP functional and def-TZVPP basis set on all atoms.

Synthesis of 2•Cl_2. The title compound was synthesized with slight modification of literature procedure.[32] To a solution of the zinc complex **1** (2.5 g, 2.74 mmol) in 50 mL of dry toluene in a Schlenk flask, PCl_3 (2.4 mL, 27.4 mmol) was added dropwise at room temperature with vigorous stirring. After stirring for 2 h at room temperature under nitrogen, the solvent was removed *in vacuo* leaving a purple solid. The solid was triturated with pentane, filtered and the solvent was removed. The light purple solid was dissolved in a minimal amount of pentane and put into the freezer at -35 °C. The product precipitated from solution as a white solid (2.1 g, 73%). ^{1}H NMR ($CDCl_3$, 360 MHz) δ/ppm: 7.58 (s, 2H), 7.07 (s, 2H), 1.43 (s, 18H), 1.39 (s, 18H). ^{31}P NMR ($CDCl_3$, 145 MHz) δ/ppm: -20.1.

Synthesis of 2•Ph_2. To a solution of the zinc complex **1** (1 g, 1.1 mmol) in 50 mL of dry toluene in a Schlenk flask, Ph_2PCl (406 μL, 2.2 mmol) was added dropwise at room temperature with vigorous stirring. After stirring for 4 h at room temperature under nitrogen, the solvent was removed *in vacuo* leaving a purple solid. The solid was triturated with cold pentane, filtered and the solvent was removed. The light purple solid was dissolved in a minimal amount of pentane and put into the freezer at -35 °C. The product precipitated from solution as a white solid (1.05 g, 79%). Single crystals of the product were grown by slow evaporation of an acetonitrile/dichloromethane solution. ^{1}H NMR (CD_2Cl_2, 500 MHz) δ/ppm: 7.80 (d, *J* = 7.0 Hz, 2H), 7.77 (d, *J* = 7.2 Hz, 2H), 7.62 (s, 2H), 7.45-7.40 (m, 2H), 7.40-7.34 (m, 4H), 6.94 (s, 2H), 1.38 (s, 18H), 1.31 (s, 18H). ^{13}C NMR (CD_2Cl_2, 126 MHz) δ/ppm: 143.93 (d, *J* = 4.4 Hz), 142.32, 140.84, 139.42, 132.04 (d, *J* = 12.1 Hz), 131.15 (d, *J* = 3.6 Hz), 129.02 (d, *J* = 19.6 Hz), 128.23 (d, *J* = 16.3 Hz), 116.35, 107.13 (d, *J* = 13.0 Hz), 35.31, 34.71, 32.13, 30.05. ^{31}P NMR ($CDCl_3$, 145 MHz) δ/ppm: -27.9. HRMS (EI^+) *m/z* calcd for $C_{40}H_{50}NO_2P$: 607.3579; found: 607.3573. Anal. Calcd (Found) for $C_{40}H_{50}NO_2P$: C 79.0 (78.9); H 8.3 (8.1); N 2.30 (2.5); P 5.1 (5.4).

Synthesis of [2•Ph_2]BF_4 (4). Compound **2**•Ph_2 (400 mg, 0.66 mmol) was dissolved in 8 mL of dry CH_2Cl_2 and was added to a solution of $AgBF_4$ (128 mg, 0.66 mmol) dissolved in 8 mL of CH_2Cl_2. The reaction stirred at room temperature for 4h and was filtered and the solvent was removed under reduced pressure. The resulting dark blue solid was washed with pentane and dried to give the title compound (420 mg, 92%). HRMS (EI^+) *m/z* calcd for $C_{40}H_{50}NO_2P$: 607.3579; found: 607.3577. Anal. Calcd (Found) for $C_{40}H_{50}BF_4NO_2P$: C 69.2 (68.8); H 7.3 (7.3); N 2.0 (2.0).

Synthesis of [2•Ph_2]$B(3,5\text{-}(CF_3)_2\text{-}C_6H_3)_4$. Compound **2**•$Ph_2$ (200 mg, 0.33 mmol) was dissolved in 4 mL of dry CH_2Cl_2 and was added to a solution of $AgB[3,5\text{-}(CF_3)_2\text{-}C_6H_3]_4$ (320 mg, 0.33 mmol) dissolved in 4 mL of CH_2Cl_2. The reaction stirred at room temperature for 4h and was filtered and the solvent was removed under reduced pressure. The resulting dark blue solid was washed with pentane and dried to give the title compound (400 mg, 82%). Single crystals suitable for x-ray diffraction were prepared by slow evaporation of a 1:3 mixture of diethylether and pentane.

ASSOCIATED CONTENT

Supporting Information

^{1}H, ^{13}C, and ^{31}P NMR spectra for all synthetic compounds; EPR spectra including spectral simulations; crystallographic and computational details. The Supporting Information is available free of charge on the ACS Publications website.

AUTHOR INFORMATION

Corresponding Author

* radosevich@mit.edu

ACKNOWLEDGMENT

We thank the NSF (CHE- 1724505) for financial support. A.T.R gratefully acknowledges additional support from the Alfred P. Sloan Foundation and Amgen. We thank Dr. Peter Mueller (MIT) for assistance with refinement of diffraction data.

REFERENCES

[1] Kaim, W.; Paretzki, A. *Coord. Chem. Rev.* **2017**, doi: 10.1016/j.ccr.2016.12.008.

[2] Broere, D. L. J.; Plessius, R.; Vlugt, J. I. van der *Chem. Soc. Rev.* **2015**, *44*, 6886–6915.

[3] Blackmore, K. J.; Ziller, J. W.; Heyduk, A. F. *Inorg. Chem.*, **2005**, *44*, 5559.

[4] Haneline, M. R.; Heyduk, A. F. *J. Am. Chem. Soc.*, **2006**, *128*, 8410.

[5] Zarkesh, R. A.; Ziller, J. W.; Heyduk, A. F. *Angew. Chem. Int. Ed.*, **2008**, *47*, 4715.

[6] Lyaskovskyy, V.; de Bruin, B. *ACS Catalysis*, **2012**, *2*, 270.

[7] Praneeth, V. K. K.; Ringenberg, M. R.; Ward, T. R. *Angew. Chem. Int. Ed.*, **2012**, *51*, 10228.

[8] Luca, O. R.; Crabtree, R. H. *Chem. Soc. Rev.*, **2013**, *42*, 1440.

[9] Chirik, P. J. *Acc. Chem. Res.* **2015**, *48*, 1687–1695.

[10] Blanchard, S.; Derat, E.; Desage-El Murr, M.; Fensterbank, L.; Malacria, M.; Mouriès-Mansuy, V. *Eur. J. Inorg. Chem.* **2012**, *2012*, 376–389.

[11] Stegmann, H. B.; Scheffler, K.; Stocker, F. *Angew. Chem. Int. Ed.* **1970**, *9*, 456.

[12] Stegmann, H. B.; Scheffler, K. *Chem. Ber.* **1970**, *103*, 1279-1285.

[13] Stegmann, H. B.; Scheffler, K.; Stocker, F. *Angew. Chem. Int. Ed.* **1970**, *10*, 499-500.

[14] Zarkesh, R. A.; Heyduk, A. F. *Organometallics*, **2009**, *28*, 6629.

[15] Heyduk, A. F.; Zarkesh, R. A.; Nguyen, A. I. *Inorg. Chem.*, **2011**, *50*, 9849.

[16] Zarkesh, R. A.; Heyduk, A. F. *Organometallics*, **2011**, *30*, 4890.

[17] Hananouchi, S.; Krull, B. T.; Ziller, J. W.; Furche, F.; Heyduk, A. F. *Dalton Trans.*, **2014**, *43*, 17991.

[18] Piskunov, A. V.; Sukhoshkina, O. Yu.; Smolyaninov, I. V. *Zhurnal Obshchei Khimii*, **2010**, *80*, 629.

[19] Shekar, S.; Brown, S. N. *Organometallics*, **2013**, *32*, 556.

[20] Turek, J.; Kampová, H.; Padělková, Z.; Růžička, A. *J. Organomet. Chem.*, **2013**, *745*, 25.

[21] Shekar, S.; Brown, S. N. *J. Org. Chem.*, **2014**, *79*, 12047.

[22] McGarvey, B. R.; Ozarowski, A.; Tian, Z.; Tuck, D. G. *Can. J. Chem.*, **1995**, *73*, 1213.

[23] Camacho-Camacho, C.; Tlahuext, H.; Nöth, H.; Contreras, R. *Heteroatom Chem.*, **1998**, *9*, 321.

[24] Camacho-Camacho, C.; Majangos, E.; Castillo-Ramos, M. E.; Esparza-Ruiz, A.; Vásquez-Badillo, A.; Nöth, H.; Flores-Parra, A.; Contreras, R. *J. Organomet. Chem.*, **2010**, *695*, 833.

[25] Ohkata, K.; Yano, T.; Kuwaki, K.; Akiba, K. *Chemistry Letters*, **1990**, 1721.

[26] Poddel'sky, A. I.; Somov, N. V.; Kurskii, Y. A.; Cherkasov, V. K.; Abakumov, G. A. *J. Organomet. Chem.*, **2008**, *693*, 3451.

[27] Poddel'sky, A. I.; Vavilina, N. N.; Somov, N. V.; Cherkasov, V. K.; Abakumov, G. A. *J. Organomet. Chem.*, **2009**, *694*, 3462.

[28] Smolyaninov, I. V.; Poddel'skii, A. I.; Berberova, N. T. *Elektrokhimiya*, **2011**, *47*, 1295.

[29] Smolyaninov, I. V.; Poddel'sky, A. I.; Smolyaninova, S. I.; Berberova, N. T. *Koordinatsionnaya Khimiya*, **2014**, *40*, 608.

[30] Chaudhuri, P.; Hess, M.; Weyhermüller, T.; Wieghardt, K. *Angew. Chem. Int. Ed.* **1999**, *38*, 1095–1098.

[31] McCarthy, S. M.; Lin, Y.-C.; Devarajan, D.; Chang, J. W.; Yennawar, H. P.; Rioux, R. M.; Ess, D. H.; Radosevich, A. T. *J. Am. Chem. Soc.* **2014**, *136*, 4640–4650.

[32] Zhao, W.; McCarthy, S. M.; Lai, T. Y.; Yennawar, H. P.; Radosevich, A. T. *J. Am. Chem. Soc.* **2014**, *136*, 17634–17644.

[33] Robinson, T. P.; De Rosa, D. M.; Aldridge, S.; Goicoechea, J. M. *Angew. Chem., Int. Ed.* **2015**, *54*, 13758–13763.

[34] Robinson, T. P.; Lo, S.-K.; De Rosa, D.; Aldridge, S.; Goicoechea, J. M. *Chem. - Eur. J.* **2016**, *22*, 15712–15724.

[35] Camacho-Camacho, C.; Martinez-Martinez, F. J.; Rosales-Hoz, M. J.; Contreas, R. *Phosphorus, Sulfur Silicon Relat. Elem.* **1994**, *91*, 189.

[36] Girgis, A. Y.; Balch, A. L. *Inorg. Chem.* **1975**, *14*, 2724.

[37] Connelly, N. G.; Geiger, W. E. *Chem. Rev.* **1996**, *96*, 877.

[38] M. Geoffroy, *Applications of EPR in Radiation Research*, ed. A. Lund and M. Shiotani, Springer International Printing, New York, 2014, Chapter 2, 33-67.

[39] Jameson, D. L.; Anand, R. *J. Chem. Ed.*, **2000**, *77*, 88.

[40] Pangborn, A. B.; Giardello, M. A.; Grubbs, R. H.; Rosen, R. K.; Timmers, F. J. *Organometallics*, **1996**, *15*, 1518.

[41] Alaimo, P. J.; Peters, D. W.; Bergman, R. G. J. *J. Chem. Ed.*, **2001**, *78*, 64.

[42] Hayashi, Y.; Rohde, J. J.; Corey, E. J. *J. Am. Chem. Soc.* **1996**, *118*, 5502.

[43] Stroll, S.; Schweiger, A. *J. Magn. Reson.* **2006**, *178*, 42.

[44] Dolomanov, O. V.; Bourhis, L. J.; Gildea, R. J.; Howard, J. A. K.; Puschmann, H. *J. Appl. Cryst.* **2009**, *42*, 339.

[45] Sheldrick, G. M *Acta Cryst.* **2008**, *A64*, 112.

[46] Frisch, M. J.; Trucks, G. W.; Schlegel, H. B.; Scuseria, G. E.; Robb, M. A.; Cheeseman, J. R.; Scalmani, G.; Barone, V.; Mennucci, B.; Petersson, G. A.; Nakatsuji, H.; Caricato, M.; Li, X.; Hratchian, H. P.; Izmaylov, A. F.; Bloino, J.; Zheng, G.; Sonnenberg, J. L.; Hada, M.; Ehara, M.; Toyota, K.; Fukuda, R.; Hasegawa, J.; Ishida, M.; Nakajima, T.; Honda, Y.; Kitao, O.; Nakai, H.; Vreven, T.; Montgomery, Jr., J. A.; Peralta, J. E.; Ogliaro, F.; Bearpark, M.; Heyd, J. J.; Brothers, E.; Kudin, K. N.; Staroverov, V. N.; Keith, T.; Kobayashi, R.; Normand, J.; Raghavachari, K.; Rendell, A.; Burant, J. C.; Iyengar, S. S.; Tomasi, J.; Cossi, M.; Rega, N.; Millam, J. M.; Klene, M.; Knox, J. E.; Cross, J. B.; Bakken, V.; Adamo, C.; Jaramillo, J.; Gomperts, R.; Stratmann, R. E.; Yazyev, O.; Austin, A. J.; Cammi, R.; Pomelli, C.; Ochterski, J. W.; Martin, R. L.; Morokuma, K.; Zakrzewski, V. G.; Voth, G. A.; Salvador, P.; Dannenberg, J. J.; Dapprich, S.; Daniels, A. D.; Farkas, O.; Foresman, J. B.; Ortiz, J. V.; Cioslowski, J.; Fox, D. J. *Gaussian 09, Revision C.01*, Gaussian, Inc., Wallingford CT, 2010.

For Table of Contents Only

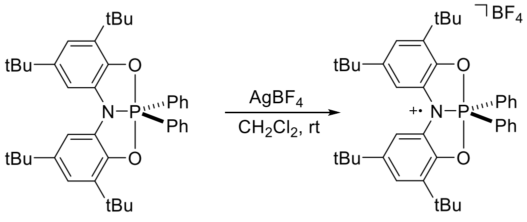

2•Ph$_2$ [**2**•Ph$_2$]BF$_4$

Synopsis: A stable open-shell phosphorane based on a redox active amidodiphenoxide scaffold may be accessed by (electro)chemical oxidation of the closed-shell congener. Spectroscopic investigations indicate that the oxidation is largely localized on the amidodiphenoxide supporting framework.